ELSEVIER

Available online at www.sciencedirect.com

SCIENCE DIRECT

Journal of Crystal Growth 249 (2003) 251–261

JOURNAL OF CRYSTAL GROWTH

www.elsevier.com/locate/jcrysgro

Surface morphology and crystallinity control in the atomic layer deposition (ALD) of hafnium and zirconium oxide thin films

Dennis M. Hausmann, Roy G. Gordon*

Harvard University Chemical Laboratories, Cambridge, MA 02138, USA

Received 28 March 2002; accepted 13 June 2002
Communicated by R.S. Feigelson

Abstract

Hafnium and zirconium oxide films were prepared by atomic layer deposition (ALD) from dialkylamido precursors. Water was used as the oxygen source. Nanolaminates of hafnium, zirconium and aluminum oxide were also prepared. Atomic force microscopy was used to characterize the surface morphology of 10–100 nm thick films grown from 50°C to 300°C. X-ray diffraction was used to characterize the film crystallinity. Transmission electron microscopy was used to relate the surface morphology to the film crystallinity. A model for the nucleation and growth of crystallites during an ALD deposition leading to surface roughness is developed based on these findings. Analysis of the film properties in the context of this model suggested nanolaminate strategies that can control the surface roughness and crystallite sizes of ALD films.
© 2002 Elsevier Science B.V. All rights reserved.

PACS: 68.60.−p; 77.55.+f; 78.20.−e; 79.60.Dp

Keywords: A3. Atomic layer epitaxy; A3. Metalorganic chemical vapor deposition; A3. Polycrystalline deposition; B1. Oxides

1. Introduction

Hafnium and zirconium oxide (HfO_2 and ZrO_2) have been extensively studied for use as a silicon dioxide (SiO_2) replacement in the gate-oxide insulating layer in complementary metal oxide semiconductor (CMOS) devices [1]. The same properties endowed upon zirconium and hafnium oxide which make them leading candidates for a gate oxide replacement also give them high potential for application as an insulating dielectric in the capacitive element in many memory devices such as DRAM [2]. These materials are also of interest in thin-film electroluminescent (TFEL) applications [3,4]. Capacitors made of a high-k dielectric film for use in such applications need to have smooth, uniform surfaces to achieve a homogeneous electric field distribution through the capacitive element. Atomic layer deposition (ALD) is an ideal method for depositing smooth

*Corresponding author.
E-mail address: gordon@chemistry.harvard.edu (R.G. Gordon).

0022-0248/03/$ - see front matter © 2002 Elsevier Science B.V. All rights reserved.
PII: S0022-0248(02)02133-4

films and it offers the additional benefit of high conformality, precise thickness control and precise composition control [5]. Films prepared by the ALD method are generally smooth for amorphous films and for single-crystal epitaxial films (polycrystalline films often have roughness due to growth of facets on the crystallites) [6]. In addition to smoothness, amorphous films may lack the high leakage current that has been associated with the grain boundaries of highly crystalline films [7,8]. However, in a capacitive role, polycrystalline films may be preferable to amorphous films due to their higher density and higher dielectric constant. Provided the resulting film is relatively smooth, polycrystalline films could still be used in capacitive applications if the crystallites in the film are much smaller than the film thickness so that grain boundaries do not extend through the thickness of the film. Inhibition of crystallite nucleation and retardation of crystallite growth are two general strategies to control film crystallinity and the crystallinity-associated surface roughness.

Published ALD preparations of both hafnium and zirconium oxide tend to produce films that are highly crystalline (with associated surface roughness) as deposited from chloride [9–12] and iodide [13,14] precursors. Prevention of the formation of crystallites can be accomplished if the depositions are run at low temperatures; however halide precursors (chloride and iodide) leave unacceptable levels of impurities at low deposition temperatures [10,13,15]. Besides low temperature deposition, crystallite growth and the associated surface roughness also can be inhibited with the periodic introduction of a second metal oxide that produces an amorphous layer in between several polycrystalline regions (a nanolaminate structure). Several reports indicate a reduction in hafnium and zirconium oxide thin film crystallinity and consequent roughness using tantalum oxide in a nanolaminate strategy [8,16,17].

To achieve low temperature deposition of pure films, very reactive precursors with completely self-limiting surface reactions are needed. Compared to metal halides, metal amides are significantly more reactive toward a hydroxylated surface (like the native oxide on silicon) since the metal–halide bond is significantly stronger than the metal–nitrogen bond (both weaker than the metal–oxygen bond) [18]. Alkyl amides of zirconium and hafnium have been known for over four decades [19], are thermally stable [20] and have sufficient volatility to be used in a vapor deposition process [19,21]. The goal of this study was to investigate the ALD deposition of zirconium and hafnium oxide using tetrakis(dimethylamido) hafnium (IV) and tetrakis(dimethylamido) zirconium (IV) in the context of film morphology and crystallinity. Besides low temperature deposition, inhibition of hafnium and zirconium oxide crystallite growth at higher temperature is investigated in this report using aluminum oxide nanolaminates. Aluminum oxide films are generally amorphous as deposited and crystalline aluminum oxide does not grow epitaxially on hafnium or zirconium oxide [16,22,23].

2. Experiment

2.1. Reactor description

ALD depositions were carried out in a flow reactor (Fig. 1). The reactor was a stainless-steel tube (76 cm in length and 3.7 cm inside diameter) heated in a tube furnace. Precursor vapors and nitrogen gas were introduced into the reactor

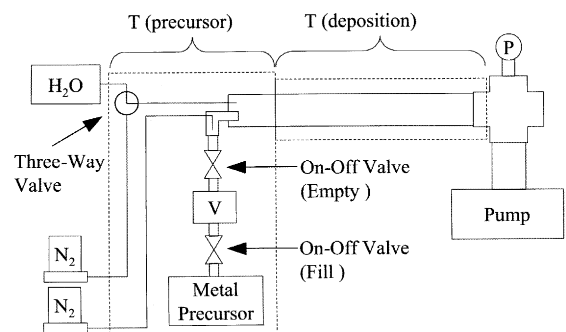

Fig. 1. Schematic diagram of the deposition system showing the location of the nitrogen mass flow controllers (N_2), the water vapor reservior (H_2O), the metal precursor reservoir (metal Precursor), the three-way gas-chromatography valve, the two on–off diaphragm valves, the metal precursor does volume (V), the pressure measurement location (P), and the rotary vane pump (Pump) with respect to the precursor (T(precursors) and deposition (T(deposition)) heating zones.

through a bored out flange at one end of the tube. Nitrogen gas was purified using Millipore inert gas purifier model VPMV200SI, rated to reduce water and oxygen to less than 1 ppb. Unreacted precursors and reaction products were removed through the opposite end (exhaust) of the reactor with a rotary vane vacuum pump. Substrates were also introduced into and removed from the reactor via a removable flange at the exhaust end of the reactor. Precursors were introduced into the reactor at the beginning of this heated zone. A 12 cm long static mixer was placed before a substrate holder. The substrate holder was a half round (32 cm in length, 3.6 cm in diameter) aluminum block. Under deposition conditions, material was deposited on all surfaces in this region. Trimethylaluminum was purchased from Albemarle Chemicals. Tetrakis(dimethylamido) hafnium (IV) and tetrakis(dimethylamido) zirconium (IV) were purchased from Aldrich Chemical Company. Prior to use in a deposition experiment, 1 ml of precursor was transferred to and stored in a 100 ml stainless-steel reservoir under a nitrogen atmosphere.

During a metal precursor dose, 10 ml of metal amide vapor was introduced into the reactor through an electronically controlled diaphragm valve (referred to as the empty valve) (see Fig. 1). A separate electronically controlled diaphragm valve (referred to as the fill valve) separated the defined volume from the precursor reservoir. This assembly (empty valve, fill valve and precursor reservoir) was heated in an oven to a temperature such that the precursor attained a vapor pressure of at least 1 Torr. Prior to opening the fill valve, the empty valve was opened to reduce the pressure in the volume between the two valves. Opening the fill valve for 1 s (while the empty valve is closed) charged the volume between the two valves with a known volume of vapor (10 ml) at a known temperature and pressure (and thus a known number of moles). Opening of the empty valve for 1 s (while the fill valve is closed) emptied this dose into the reactor, which was at a pressure well below 1 Torr. Nitrogen gas flow (constant during the deposition) was directed at the reactor side end of the empty valve to assist in the complete emptying of the vapor space.

Water and trimethylaluminum vapors were each introduced into the reactor by the action of two separate three-way gas-chromatography (GC) valves connected to the reactor by two stainless-steel feed-throughs (0.04 cm inner diameter). The GC valves were controlled electronically and could be positioned in two states to allow either nitrogen gas (purge state) or vapor (dose state) to flow into the reactor. The water vapor was kept at room temperature and thus had a vapor pressure of approximately 24 Torr. The trimethylaluminum vapor was also kept at room temperature and thus had a vapor pressure of approximately 16 Torr. A single saturating dose consisted of positioning the GC valve in the dose state for $\frac{1}{2}$ a second and then returning it to the purge state. The GC valve was always kept (during the deposition) in the purge state except during the dose time intervals.

During a deposition experiment, the total nitrogen mass flow into the reactor was 0.025 standard liters per minute (SLPM) and the pressure of nitrogen in the reactor was maintained at 0.25 Torr (gas molecules had an average linear flow velocity of 300 cm/s in the reactor at 200°C). The deposition temperature was varied from 50°C to 350°C. At least 5 s of purging was allowed between the doses of precursors. Under these conditions one ALD reaction cycle was defined as one dose of the metal precursor followed by a 5 s purge, then one dose of water followed by another 5 s purge. At all times during the deposition, nitrogen flow was kept constant. During a purge, no precursors were introduced into the reactor.

All substrates were exposed to a UV lamp (in air to generate ozone) for 3 min (sufficient to restore the hydrophilic character of a HF dipped silicon wafer) immediately prior to deposition. Silicon substrates were cut from prime grade wafers (1 0 0) and cleaned in a 48% HF solution for 5 s prior to UV/Ozone treatment. Quartz substrates, for XRD analysis, were purchased from the Gem Dugout, and were cut 6° from (0 0 0 1) to ensure a low background. TEM analysis was performed on silicon as well as thin carbon thin films on 200 mesh copper grids purchased from Ernest F. Fullam Inc.

The phase and crystallinity of the films were determined by powder X-ray diffraction (XRD) using a Scintag XDS 2000 instrument with Cu Kα radiation (1.54 nm wavelength). High angle XRD data was collected at 0.02° increments and 10 s count times using films deposited on both quartz and silicon substrates. Scherrer's method was used to find the average height of crystallites [24].

Phase and crystallinity data were also obtained using a JEOL 2010F high resolution transmission electron microscope (HRTEM). A two-dimensional Fourier transform (FFT) was obtained for all collected data. HRTEM samples on silicon were prepared by dimpling the sample, followed by mechanical polishing, and finally ion-milling of the substrate to produce a thin-foil of the film. HRTEM samples on carbon were used as deposited. Local heating of the samples to observe in situ crystallization of amorphous samples was induced by focusing down the electron beam until lattice planes could be clearly observed (typically a few minutes).

The surfaces of the films deposited on silicon were analyzed with a Nanoscope VI (Digital Instrument) atomic force microscope (AFM) with a silicon tip (10 nm radius of curvature) in the tapping mode. 1.0 μm areas were scanned at a rate of 2 Hz at a resolution of 8-bits. The rms-roughness of the silicon substrates ranged from 0.15 to 0.20 nm before deposition.

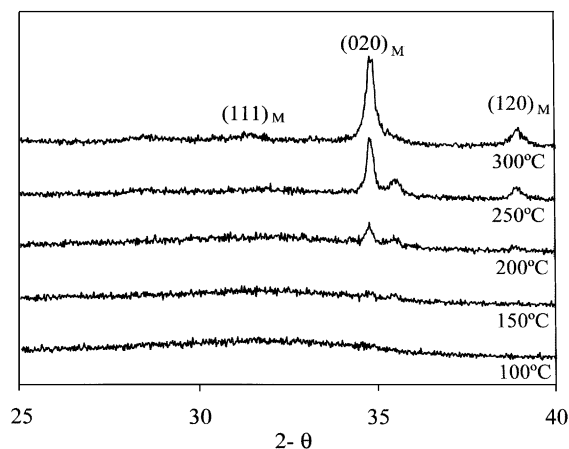

Fig. 2. A portion of the XRD spectrum for 100 nm-thick hafnium oxide films deposited at several different deposition temperatures.

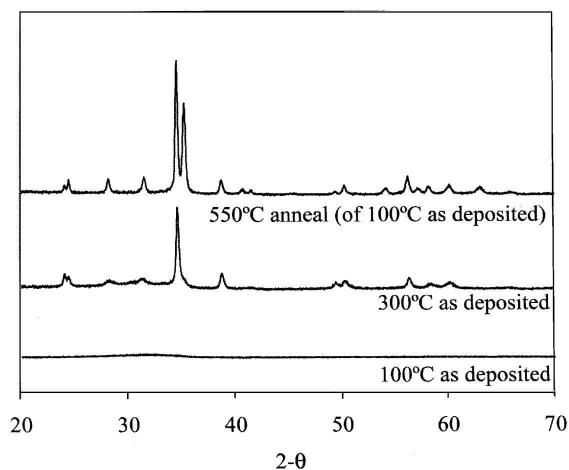

Fig. 3. The XRD spectra for 100 nm-thick hafnium oxide films deposited at 100°C, deposited at 300°C, and the annealed film deposited at 100°C.

2.2. Film characterization: X-ray diffraction

XRD spectra recorded on 100 nm thick as-deposited hafnium oxide films at several deposition temperatures are shown in Fig. 2. At deposition temperatures less than 100°, no peaks are observed (consistent with an amorphous film), while at higher deposition temperatures peaks are observed and increased in intensity as the deposition temperature was increased. The observed peaks are consistent with the monoclinic crystalline phase. The film deposited at 100°C was annealed at 550°C for 2 h, under a dynamic vacuum (0.02 Torr). Peaks were observed consistent with the monoclinic phase (Fig. 3) in this film. The relative intensities of these peaks were different from the film deposited at higher temperatures (and subject to no annealing); the peak intensities observed in the annealed film's XRD pattern were identical to those observed in the powder pattern of monoclinic hafnium oxide. The same result was obtained from annealing at 750°C for 1 m, and annealing at 1000°C for 10 s both under a dynamic vacuum (0.02 Torr).

Similar results were observed for the zirconium oxide films (Fig. 4). The peaks in the XRD Spectra

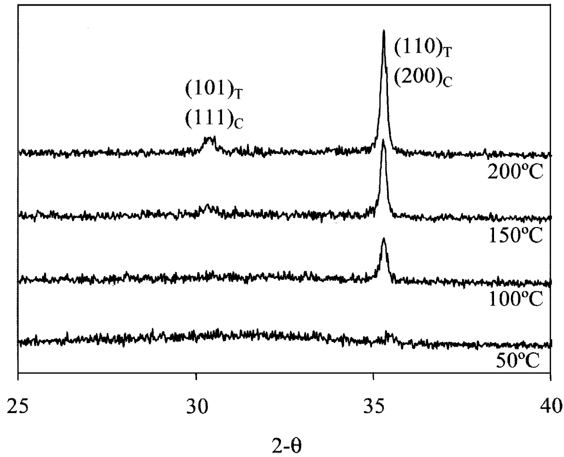

Fig. 4. A portion of the XRD spectrum for 100 nm-thick zirconium oxide films deposited at several different deposition temperatures.

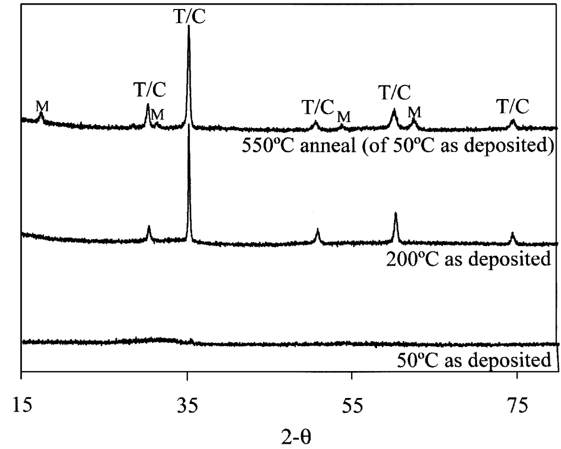

Fig. 5. The XRD spectra for 100 nm-thick zirconium oxide films deposited at 50°C, deposited at 200°C, and the annealed film deposited at 50°C.

were consistent with either the tetragonal or cubic phases. At a deposition temperature of 50°C a small peak (comparable to a peak observed in the XRD of hafnium oxide deposited at 150°C) is observed in the XRD; while mostly amorphous, this film does contain evidence of some crystallinity. The film deposited at 50°C was annealed at 550°C for 2 h, under a dynamic vacuum (0.02 Torr). Peaks were observed consistent with the monoclinic phase as well as either the tetragonal or cubic phases (Fig. 5) in this film. The same result was obtained from annealing at 750°C for 1 min, and annealing at 1000°C for 10 s both under a dynamic vacuum (0.02 Torr).

The percent crystallinity for each 100 nm-thick sample was estimated by the ratio of the area under each crystalline peak to the total area in the XRD spectra. A plot of the percent crystallinity obtained in this manner for both hafnium and zirconium oxide is shown in Fig. 6. Using Scherrer's method the average height of the crystallites was determined to be approximately 50 nm, about half of the film thickness. The full-width at half-maximum for the major peak in each XRD spectra (approximate 2θ of 35° for zirconium oxide and for hafnium oxide) for the as-deposited films was found to be largely invariant with the deposition temperature.

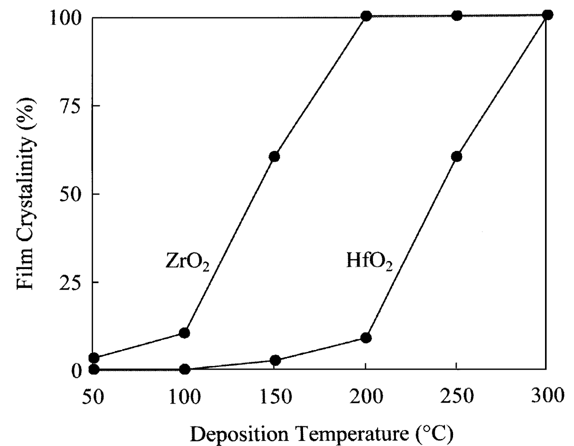

Fig. 6. The XRD determination of percent crystallinity as a function of deposition temperatures for 100 nm-thick hafnium and zirconium oxide films.

2.3. Film characterization: TEM

Low resolution TEM images of thin (thickness less than 50 nm) films of zirconium and hafnium oxide grown on carbon revealed many easily observable crystalline regions at higher deposition temperatures (Fig. 7). The crystallites were roughly spherical and evenly distributed in both size (diameter) and intensity (thickness). Scanning many such areas revealed that the largest observed

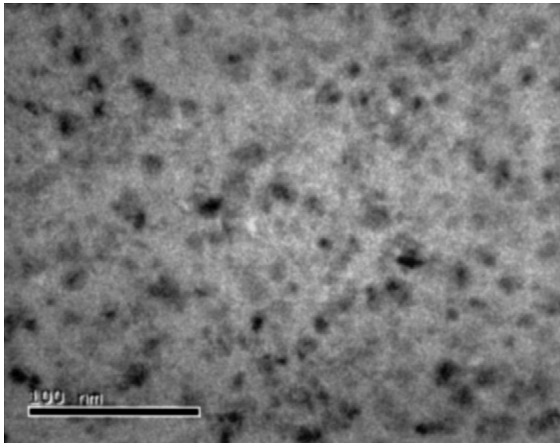

Fig. 7. Low Resolution TEM image of 50 nm-thick hafnium oxide film showing a wide distribution of crystallites sizes.

crystal diameter was always slightly less than the film thickness and the average observed crystal diameter was always slightly less than half the film thickness. A high-resolution image of one crystal on the $[1\,0\,\bar{1}]$ zone axis and its corresponding FFT (monoclinic [0 2 0] diffraction reflections) is shown in Fig. 8. The samples grown at the lower temperatures showed little that could be attributed to an ordered arrangement of atoms. Beam heating of the amorphous material produce a marked change in the high-resolution TEM image; obvious crystallization became evident.

2.4. Film characterization: AFM

AFM surface plots for several 100 nm-thick hafnium oxide films grown at several temperatures are shown in Fig. 9. AFM analysis of the as deposited hafnium oxide films showed an RMS roughness that was less than 1% of the film thickness (e.g. a smooth film) at low deposition temperatures (50°C for a 100 nm thick film). The RMS roughness reached as much as 5% for the films deposited at higher temperatures (150–250°C for the 100 nm thick film). Similar observations were made with the zirconium oxide; however roughness was observed at much lower deposition temperatures (50°C for a 100 nm thick film). There was no evidence of a surface morphology change after the annealing experiments previously dis-

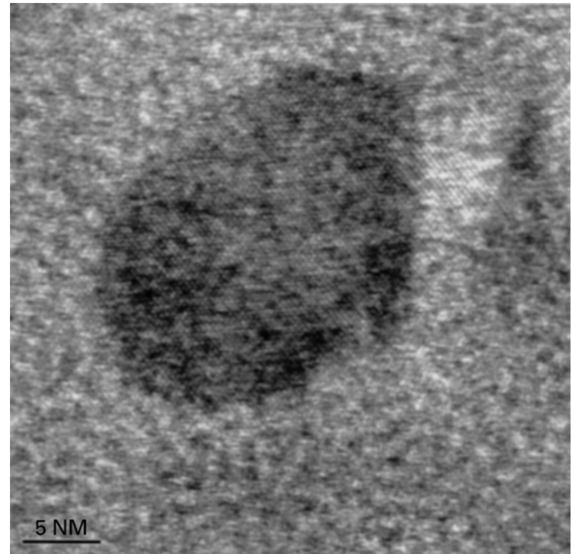

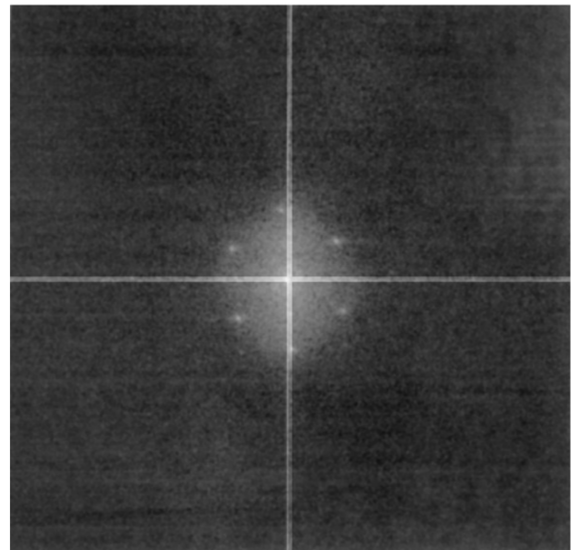

Fig. 8. High Resolution TEM image of a single crystallite and its FFT.

cussed; the films that were smooth as-deposited remained smooth after annealing.

In all cases conical features clearly seen on the surface were the cause of the surface roughness. The number density and size distribution of these features is the same as the number density and size distribution of the crystalline regions observed in TEM. From these statistics, we conclude that the features observed in the AFM images are the

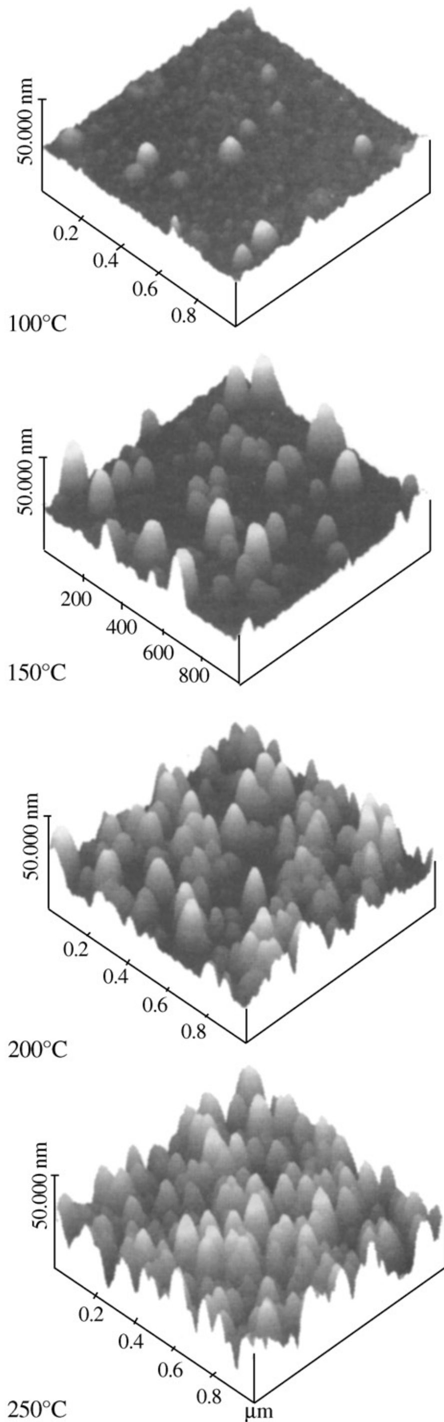

Fig. 9. AFM surface plots of 100 nm-thick hafnium oxide film as a function of deposition temperature. The scanned area is $1 \times 1\ \mu m^2$. The height scale is from 0 to 50 nm.

upper surfaces of the crystallites observed in TEM. The exposed surface of the crystallites achieved a maximum diameter equal to the film thickness. Analysis of the height and diameter of the exposed surface of the crystallites for all samples showed them to be evenly distributed in size (height and diameter).

3. Discussion

3.1. The crystal nucleation and growth model

A clearer picture of the nucleation and growth of crystals is obtained with the following model (diagrammed in Fig. 10). Nucleation events are

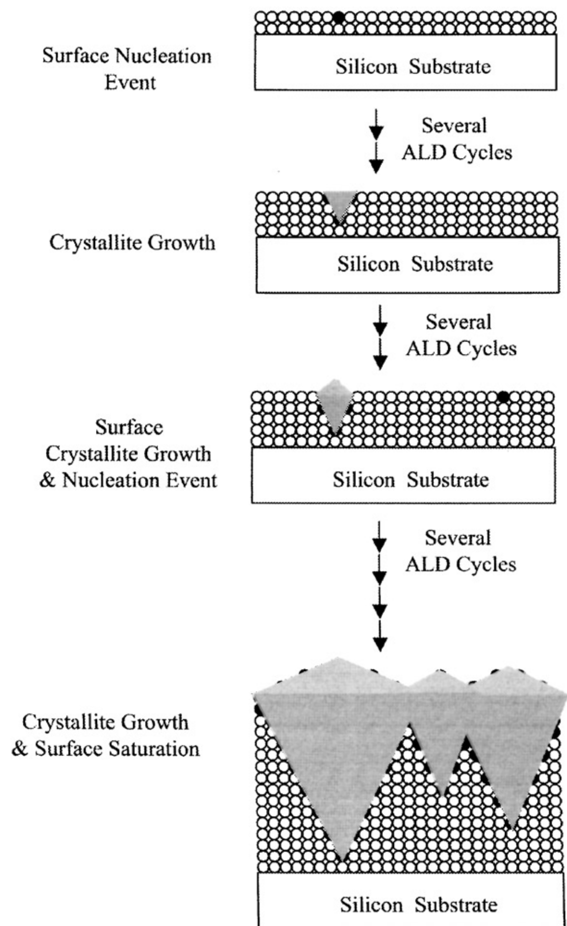

Fig. 10. The proposed crystal growth and nucleation model.

equally probable at each cycle of the film deposition; each ALD cycle allows for the possibility of one or more nucleation events randomly distributed over the surface of the amorphous regions of the film. After a nucleus has formed, the next ALD cycle contributes further mass to the nuclei resulting in a growing crystallite. The crystallite grows faster upward in the direction of the film growth and faster radially outward relative to the surrounding amorphous material. The upward growth rate is approximately 20% faster than the growth rate of the amorphous material. At higher deposition temperatures, nucleation events become more probable and thus the film becomes more crystalline. As the film grows thicker the total number of nuclei increase and the films become more crystalline due to the growth of the crystallite nuclei. At some point during the deposition process the surface becomes saturated with crystallites and further nucleation events and radial crystal growth will cease. However, vertical growth in the direction of the growing film will continue and crystallites will begin to assume a columnar structure. Each individual crystallite has a cone-like top. Since the diameter of the crystallite is approximately equal to its depth below the surface (both in terms of the maximum values and also the statistical average) the cone angle must then be approximately 53°.

3.2. Consequences of the crystal nucleation and growth model

Since every crystal observed originated from a nucleation event, the energy required for the amorphous to crystalline phase transition can be determined by counting the number of crystallites nucleated per cm^2 per ALD cycle at different temperatures (Fig. 11). Arrhenius behavior is clearly observed with activation energy equal to 38 kJ/mol. Similar behavior was observed with zirconium oxide; however the activation energy was lower, 24 kJ/mol.

AFM complements the XRD measure of film crystallinity. If the observed surface crystallite has a cone-like structure depicted by this model then the volume occupied by the crystallite is one-third the volume occupied by a cylinder with the same

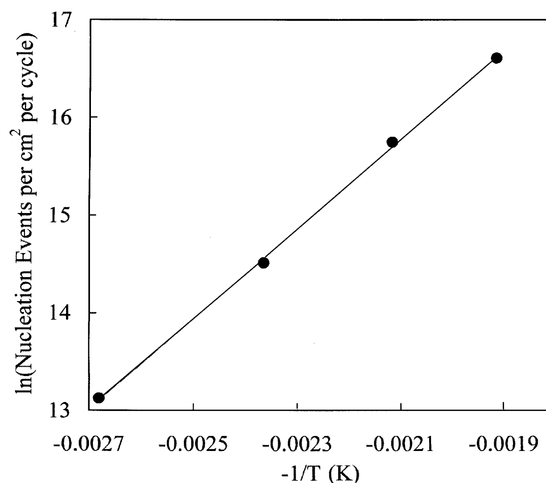

Fig. 11. Rate of hafnium oxide crystallite nucleation as a function of deposition temperature.

diameter. Due to the uniform distribution of nucleation events during the growth of the film, the average fraction of volume occupied by crystallites will be three-fourths the average fraction of surface area occupied by crystallites. Thus the volume percent crystallinity can be estimated asone-fourth the percent of the total surface area occupied by crystallites. The important assumption in this measure of crystallinity is that no crystallite is covered by another crystallite; every crystallite must clearly be observable from the surface of the film. This is only the case if the crystallites do not completely cover the surface, which would correspond to a crystallinity of at most 25% when the surface is saturated by crystallites. A comparison of crystallinity determined using this method and determined using XRD is shown in Fig. 12. The values show the same trends, but the XRD values are systematically lower probably because of the difficulty in finding the base line for the XRD data, and the AFM values are systematically higher probably due to the finite tip diameter, which will tend to exaggerate the size of the crystallites.

For some electrical and optical applications, smooth films are generally more desirable than rough films. This model of crystal nucleation and growth suggests that smooth films of materials that tend to crystallize readily during the deposi-

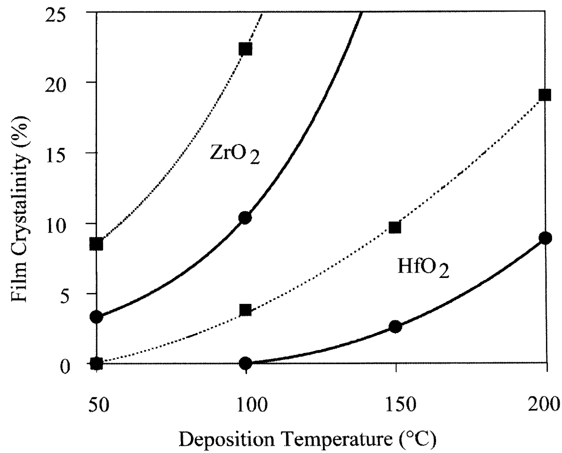

Fig. 12. Film Crystallinity as a function of deposition temperature for both hafnium and zirconium oxide determined by AFM (dashed lines) and XRD (solid lines). (Lines are drawn in for clarity).

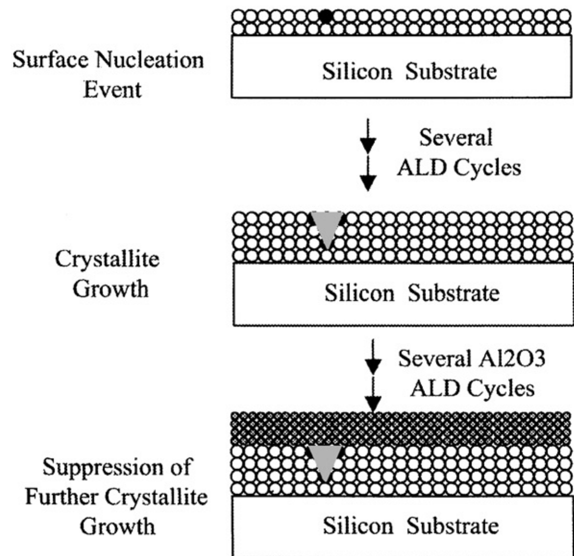

Fig. 13. A model of the nanolaminate strategy used to retard crystal growth.

tion process can be attained if nuclei formation and crystal growth are inhibited. As has already been shown, lowering the deposition temperature reduces the energy available for atoms to nucleate on the film surface and produces films with lower crystallinity and smoother surfaces.

3.3. Nanolaminates in the context of the crystal nucleation and growth model

At higher deposition temperatures, the growth of crystallites after the nucleation event has occurred can be prevented with nanolaminate structures (atomic material layers). This strategy (diagrammed in Fig. 13) requires that the second material being deposited does not nucleate and grow crystallites. When a second material is deposited on top of the growing crystallites, crystallite growth will cease if the second material does not crystallize epitaxially on top of the preexisting crystallites. By atomic material layers, the size of the crystallites can be effectively capped. However it should be noted that this strategy is dependent on the materials forming the alternating layers not crystallizing epitaxially. In the case of alternating layers of hafnium oxide and zirconium oxide, crystal growth would not be retarded since both can adopt a monoclinic or tetragonal phase with very similar lattice parameters. In addition, both hafnium and zirconium oxide contribute appreciable nucleation events to the growing film. Aluminum oxide, however, does not have an epitaxial relation to that of either hafnium or zirconium oxide and thus an aluminum oxide layer on should not adopt the crystallinity of an underlying layer of crystalline zirconium or hafnium oxide, in addition at the deposition temperature under study, aluminum oxide does not grow or nucleate crystallites.

A 50 nm-thick Zirconium oxide film deposited at 200°C was used as a test for this approach to grow smooth films by preventing the growth of crystallites. A single hafnium oxide or aluminum oxide layer was introduced after every zirconium oxide layer; these films were composed of alternating ALD cycles of zirconium oxide and hafnium/aluminum oxide. Thus the composition of these nanolaminate films was about 50% (volume fraction) zirconium oxide and 50% hafnium (or aluminum) oxide. AFM plots for the pure zirconium oxide and the two nanolaminate films are shown in Fig. 14. The nanolaminate with alternating hafnium oxide and zirconium oxide layers has less roughness than the pure zirconium oxide film due to fewer crystallites. However, the

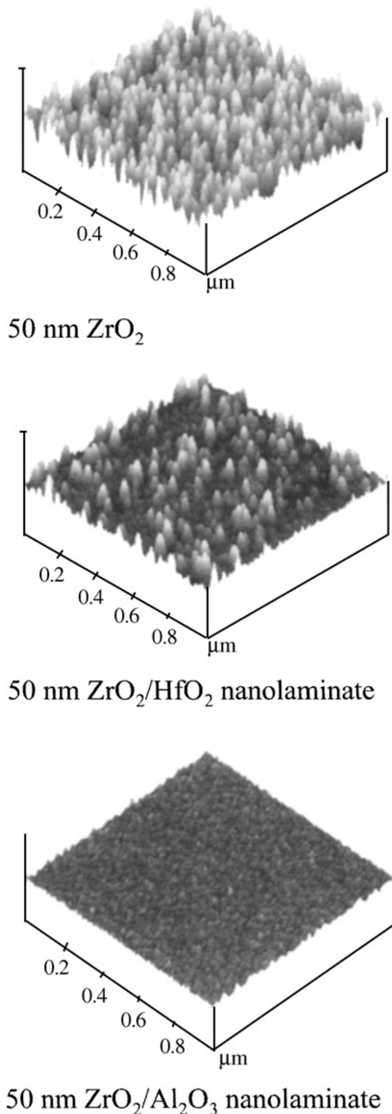

Fig. 14. AFM surface plots of a 50 nm-thick zirconium oxide film deposited at 200°C (top), 50 nm-thick zirconium/hafnium nanolaminate (middle), 50 nm-thick zirconium/aluminum nanolaminate (bottom). The scanned area is $1 \times 1\ \mu m^2$. The height scale is from 0 to 20 nm.

hafnium oxide layer did not prevent the growth of the crystallites nucleated by the zirconium oxide layer; although the number density is reduced, the height distribution is unchanged. The hafnium oxide did not contribute appreciable nucleation events to the growing film, but it did grow epitaxially on the crystallite nuclei of zirconium oxide. In the case of aluminum oxide nanolaminate, the film is completely smooth as would be expected since the aluminum oxide retards the growth of the crystallites as well as not contributing to nucleation events.

Adding a significant amount of aluminum oxide to a pure hafnium or zirconium oxide film will alter many of there desirable properties (such as the dielectric constant). The minimum number of aluminum oxide layers needed to retard crystal growth between two thicker layers of hafnium or zirconium oxide was found to be 5 (approximately 0.5 nm). 5 layers (approximately 0.5 nm) of aluminum oxide intercalated between 100 layers (approximately 10 nm) of zirconium (or hafnium) oxide were sufficient to disrupt the crystal growth from one zirconium (or hafnium) oxide layer to another and produced smoother films. The surface of this film was identical to the smooth film shown in Fig. 14.

4. Conclusions

The results reported here show that the alkyl amides of hafnium and zirconium provide convenient and effective ALD precursors to smooth, amorphous hafnium and zirconium oxide thin films. For high temperature depositions the nanolaminate strategy can be used to deposit smooth films. The model presented here is consistent with the observations and provides a clear mechanism for the nucleation and growth of crystallites during the ALD process. The few percent aluminum-oxide required to produce smooth films should not alter the bulk material properties significantly. For semiconductor applications where only a few nanometers of film are required, the alkyl-amide precursors can be used at low enough temperatures (200°C or less) where the roughening effects of crystallization are reduced and/or eliminated.

Acknowledgements

The authors are thankful to Dr. Warren MoberlyChan for insightful discussions and technical assistance with TEM.

References

[1] G.D. Wilk, R.M. Wallace, J.M. Anthony, J. Appl. Phys. 89 (2001) 5243.
[2] M. Gutsche, H. Seidl, J. Luetzen, A. Birner, T. Hecht, S. Jakschik, M. Kerber, M. Leonhardt, P. Moll, T. Pompl, H. Reisinger, S. Rongen, A. Saenger, U. Schroeder, B. Sell, A. Wahl, D. Schumann, Technical Digest International Electron Device Meeting. 18.6.1, IEEE, Piscataway, NJ, 2001.
[3] C.T. Hsu, S.W. Li, C.H. Liu, Y.K. Su, T.S. Wu, M. Yokoyama, J. Appl. Phys. 71 (1992) 1509.
[4] J.W. Li, Y.K. Su, M. Yokoyama, Jpn. J. Appl. Phys. 32 (1993) 5591.
[5] M. Leskelä, M. Ritala, J. Phys. IV France 9-Pr8 (1999) 837.
[6] C. Goodman, M. Pessa, J. Appl. Phys. 60 (1986) R65.
[7] P. Balk, J. Non-Cryst Sol. 187 (1995) 1.
[8] K. Kukli, J. Ihanus, M. Ritala, M. Leskelä, J. Electrochem. Soc. 144 (1) (1997) 300.
[9] M. Copel, M. Gribelyuk, E. Gusev, Appl. Phys. Lett. 76 (2000) 436.
[10] J. Aarik, A. Aidla, H. Mändar, V. Sammelselg, T. Uustare, J. Crystal Growth 220 (2000) 105.
[11] M. Ritala, M. Leskelä, Appl. Surf. Sci. 75 (1994) 333.
[12] M. Ritala, M. Leskalä, L. Niinistö, T. Prohaska, G. Friedbacher, M. Grasserbauer, Thin Solid Films 250 (1994) 72.
[13] K. Kukli, K. Forsgren, M. Ritala, M. Leskelä, J. Aarik, A. Hårsta, J. Electrochem. Soc. 148 (2001) 227.
[14] K. Kukli, K. Forsgren, J. Aarik, T. Uustare, A. Aidla, A. Niskanen, M. Ritala, M. Leskelä, A. Härsta, J. Crystal Growth 231 (2001) 262.
[15] J. Aarik, A. Aidla, A–.A. Kiisler, T. Uustare, V. Sammelselg, Thin Solid Films 340 (1999) 110.
[16] M. Ritala, M. Leskalä, L. Niinistö, T. Prohaska, G. Friedbacher, M. Grasserbauer, Thin Solid Films 249 (1994) 155.
[17] K. Kukli, J. Ihanus, M. Ritala, M. Leskelä, Appl. Phys. Lett. 68 (1996) 26.
[18] D.J. Cardin, M.F. Lappert, C.L. Raston, Chemistry of Organo-Zirconium and Hafnium Compounds. West Sussex, Ellis Horwood Limited, England, 1986, p. 16.
[19] D.C. Bradley, I.M. Thomas, J. Chem. Soc. 3857.\par (1960).
[20] E.I. Tsyganova, L.M. Dyagileva, Y.A. Aleksandrov, Russ. J. Chem. 69 (1999) 1532.
[21] A.M.B. van Mol, J.P.A.M. Driessen, J.L. Linden, M.H.I.M. de Croon, C.I.M.A. Spee, J.C. Schouten, Chem. Vap. Dep. 7 (2001) 101.
[22] C.M. Scanlan, M. Gajdardziska-Josifovska, C.R. Alta, Appl. Phys. Lett. 64 (1994) 3548.
[23] Y.S. Kim, J.S. Kang, S.J. Yun, K–.I. Cho, J. Kor. Phys. Soc. 35 (1999) 5216.
[24] E.W. Nuffied, X-ray Diffraction Methods. Wiley, New York, 1966, p. 147.